

# Machine Learning Quantifies Accelerated White-Matter Aging in Persons With HIV

Kalen J. Petersen,<sup>1,✉</sup> Jeremy Strain,<sup>1</sup> Sarah Cooley,<sup>1,✉</sup> Florin Vaida,<sup>2</sup> and Beau M. Ances<sup>1</sup>

<sup>1</sup>Department of Neurology, Washington University School of Medicine, St Louis, Missouri, USA; and <sup>2</sup>Department of Family and Preventive Medicine, University of California, San Diego, California, USA

**Background.** Persons with HIV (PWH) undergo white matter changes, which can be quantified using the brain-age gap (BAG), the difference between chronological age and neuroimaging-based brain-predicted age. Accumulation of microstructural damage may be accelerated in PWH, especially with detectable viral load (VL).

**Methods.** In total, 290 PWH (85% with undetectable VL) and 165 HIV-negative controls participated in neuroimaging and cognitive testing. BAG was measured using a Gaussian process regression model trained to predict age from diffusion magnetic resonance imaging in publicly available normative controls. To test for accelerated aging, BAG was modeled as an age × VL interaction. The relationship between BAG and global neuropsychological performance was examined. Other potential predictors of pathological aging were investigated in an exploratory analysis.

**Results.** Age and detectable VL had a significant interactive effect: PWH with detectable VL accumulated +1.5 years BAG/decade versus HIV-negative controls ( $P = .018$ ). PWH with undetectable VL accumulated +0.86 years BAG/decade, although this did not reach statistical significance ( $P = .052$ ). BAG was associated with poorer global cognition only in PWH with detectable VL ( $P < .001$ ). Exploratory analysis identified Framingham cardiovascular risk as an additional predictor of pathological aging ( $P = .027$ ).

**Conclusions.** Aging with detectable HIV and cardiovascular disease may lead to white matter pathology and contribute to cognitive impairment.

**Keywords.** HIV; white matter; machine learning; MRI; diffusion tensor imaging; aging; brain age.

Human immunodeficiency virus (HIV) infection is linked with accelerated age-like neurological changes at multiple scales, from epigenetics [1] to tissue microstructure [2–7] and volume [8–11]. While combination antiretroviral therapy (cART) has reduced the prevalence of severe neural injury and overt dementia, subtler white matter changes may still occur in older persons with HIV (PWH) [12]. However, imaging findings in white matter have proven heterogeneous in degree and localization.

Older PWH are a growing population, with a majority in the United States over 50 years of age [13]. This demographic shift has precipitated a new focus on clinical characterization of older PWH [14]. It is crucial to accurately measure neural aging phenotypes, quantify the contributions of non-HIV risk factors, and examine the role that predictors of risk or resilience play in neurological heterogeneity [15]. Studies of PWH must account for comorbidities, especially cardiovascular disease,

coinfections, and neurocognitive disorders, which are often confounded with primary HIV effects [16].

To address these challenges, innovative approaches are needed. Brain-predicted age is an emerging technique to quantify the effects of disease on brain health [8, 17]. This approach depends on the existence of a predictable relationship between chronological age and biological brain predicted age, estimated from age-like biomarkers. Associations between chronological age and neuroimaging features (eg, cortical thickness) are modeled in a normative population using supervised machine learning. These models are then used to test for deviation in a population of interest, which may demonstrate accelerated aging. Model residuals capture the difference between biological and chronological age, and are termed the brain-age gap (BAG). BAG provides a reproducible, prognostic summary metric of neural health [18].

Here, we apply this method to quantify the neurological effects of HIV across the lifespan. Previous work has found evidence of BAG-associated volumetric loss in PWH [19] and faster decline in cerebral blood flow with detectable viral load (VL) [20]. However, it is unknown whether similar acceleration is present in white matter microstructure.

Microstructure is quantified using diffusion tensor imaging (DTI) quantities including fractional anisotropy (FA) and mean diffusivity (MD). FA measures the directional bias of

Received 20 December 2021; editorial decision 20 April 2022; accepted 22 April 2022; published online 28 April 2022.

Correspondence: Kalen J. Petersen, PhD, Washington University in St Louis, 600 South Euclid Avenue, Box 8111, St Louis, MO 63130 (kalen@wustl.edu).

The Journal of Infectious Diseases® 2022;226:49–58

© The Author(s) 2022. Published by Oxford University Press on behalf of Infectious Diseases Society of America. All rights reserved. For permissions, please e-mail: journals.permissions@oup.com

<https://doi.org/10.1093/infdis/jiac156>

diffusion in parallel axon bundles. FA is reduced in damaged white matter, and is sensitive to axonal degeneration and altered myelination. In contrast, MD measures membrane density and is sensitive to cellularity, necrosis, and edema. Here, we applied machine learning to both FA and MD to derive BAG from white matter microstructure.

The goals of this cross-sectional study were 3-fold. First, we tested the hypothesis that age and detectable VL interact to increase the risk of elevated BAG in older PWH compared to HIV-seronegative controls. Next, we quantified the association between white matter aging and cognitive performance, and tested whether detectable VL moderates this structure-function relationship. Finally, we sought to understand aging heterogeneity among PWH by identifying comorbid clinical risk factors associated with white matter changes.

## METHODS

### Overview

DTI from a normative external dataset was used to train a machine learning model to quantify the BAG. This model was then applied to study participants, both PWH and HIV-negative controls. The resulting BAG values were then used in multivariate regression analyses of HIV serostatus, aging, VL, and other risk factors for accelerated aging and cognitive impairment (Figure 1).

### Participants

Adults with HIV were recruited from the Washington University Infectious Diseases Clinic between 2009 and 2020, and HIV-negative controls were recruited from the Research Participant Registry or community organizations. Study procedures were approved by the Institutional Review Board, and all participants provided written informed consent.

Participants were excluded for confounding neurological or psychiatric disorders, Beck Depression Inventory-II > 29, traumatic brain injury with prolonged unconsciousness, opportunistic central nervous system infection, or current substance use disorders. A urine-analysis test was administered to screen for controlled substances other than cannabis.

Current CD4 and CD8 T-cell counts were measured for PWH, and nadir CD4 values were identified from laboratory or medical records. HIV serostatus and plasma VL were assessed with reverse transcriptase-polymerase chain reaction (PCR), and seronegativity was confirmed for controls. PWH with plasma VL > 50 copies/mL were considered to have detectable VL, and analyzed separately. Hepatitis C status, ART duration, and HIV infection duration were obtained from medical records.

Body mass index and 10-year Framingham cardiovascular risk score were calculated from values recorded during the study visit. Framingham score is derived from a weighted

combination of age, total cholesterol, high density lipoprotein cholesterol, systolic blood pressure, antihypertensive use, and smoking, with different beta weights and interaction terms for men and women [21]. For participants with missing inputs (eg, cholesterol), multiple imputation from chained equations (MICE) with 5 imputations was used to estimate Framingham scores [22], as in previous studies [23, 24]. This method was validated by random deletion of 50% of data to create pseudomissing values, iterated 1000 times. True and imputed scores had a mean correlation of  $r = 0.72$  (SD 0.05).

### Cognitive Testing

Participants underwent neuropsychological testing in 5 domains: learning, delayed recall, executive function, psychomotor speed, and language, as previously described [25]. Within each domain, z-scores were calculated norming for age, sex, race, and education where applicable. Global z-scores were obtained by averaging across domains.

### Neuroimaging

Magnetic resonance imaging (MRI) was performed at 3.0 Tesla on a Tim Trio scanner (Siemens), and included T<sub>1</sub>-weighted and diffusion-weighted MRI, acquired with repetition time/echo time (TR/TE) = 9900/102 ms, spatial resolution = 2 × 2 × 2 mm, 23 gradient directions, and b-values from 0 to 1400 s/mm<sup>2</sup>.

Images were preprocessed using the FMRIB Software Library (FSL; Oxford, UK) and the ENIGMA DTI toolbox [26]. Diffusion-weighted images were brain-extracted and corrected for motion and eddy currents using *eddy\_correct*, and tensors were calculated using *DTIFIT* and registered to an FA template brain in MNI space. Tract-based spatial statistics (TBSS) were used to map FA and MD values onto a 1-mm thick white matter skeleton, reducing registration-related discrepancies by mapping the maximal FA in the vicinity onto skeletal voxels.

Mean FA and MD were extracted from skeleton voxels overlapping with 44 white matter regions-of-interest (ROIs) using the Johns Hopkins University atlas, omitting brainstem. For simplicity, white matter ROIs were reduced to 12 by averaging left and right sides and combining subregions (eg, genu + body of corpus callosum). The following ROIs were examined: cingulum, corona radiata, corpus callosum, corticospinal tract, external capsule, fornix, frontal-occipital fasciculus, internal capsule, superior longitudinal fasciculus, sagittal stratum, thalamic radiation, and uncinate fasciculus.

### Training Data

To model brain predicted age, we utilized publicly available neuroimaging from healthy individuals across the lifespan from the Cambridge Center for Ageing and Neuroscience (CamCAN) [27, 28]. CamCAN diffusion MRI was acquired

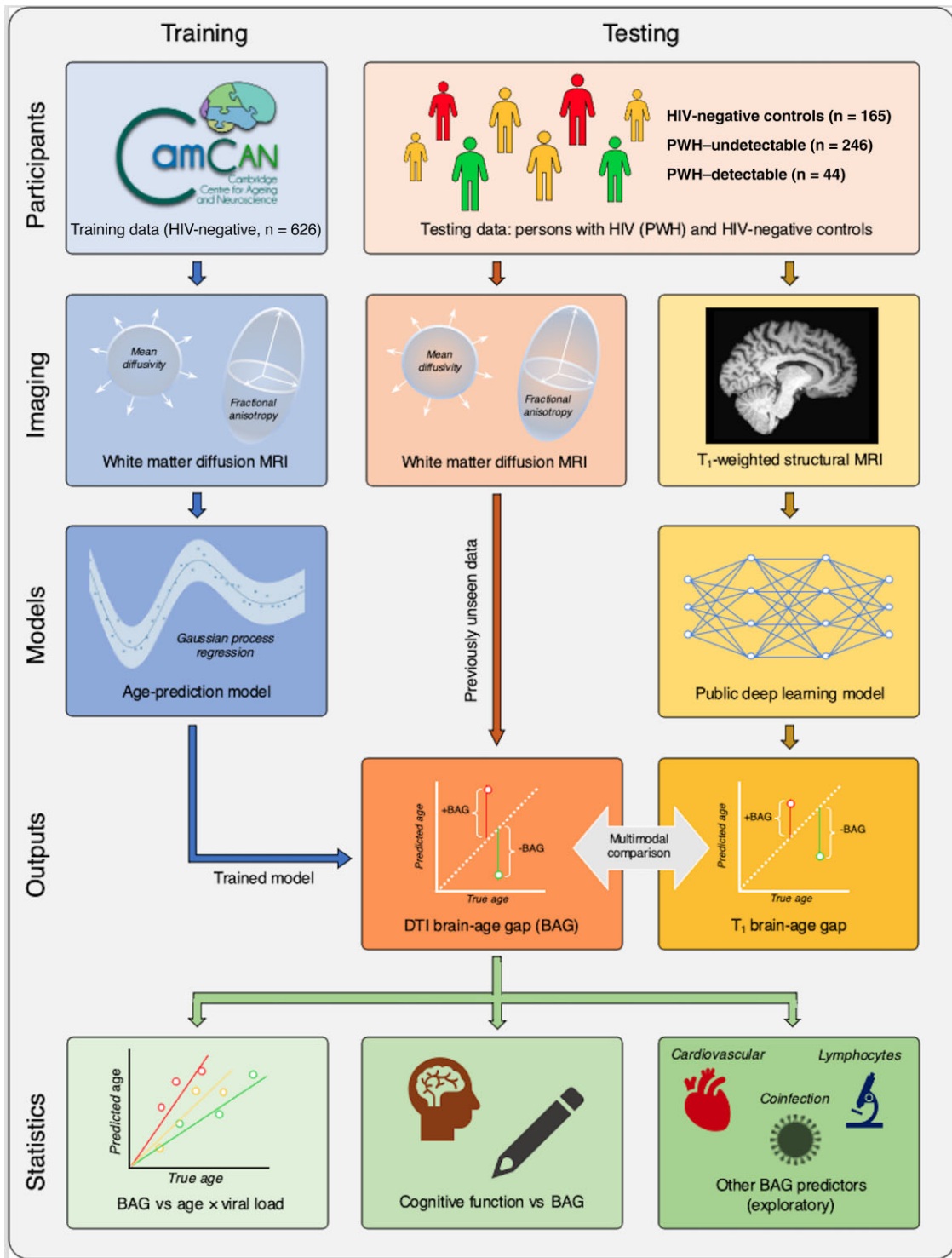


**Figure 1.** Study overview. Machine learning was used to generate the brain-age gap (BAG). Training data (left column) consisted of diffusion-weighted magnetic resonance imaging (MRI) scans from the Cambridge Center for Ageing and Neuroscience (CamCAN). Diffusion tensor metrics fractional anisotropy (FA) and mean diffusivity (MD) were calculated and used in training a Gaussian process regression machine learning model to estimate participant age from neuroimaging. Study participants (middle column) including persons with HIV (PWH) and HIV-negative controls underwent a comparable MRI protocol. Diffusion tensor metrics from these participants constituted testing data for the model. BAG, the difference between predicted and true age, was the output preserved for statistical analysis. Additionally, T<sub>1</sub>-weighted volumetric MRI (right column) from the same participants was used to generate an alternative BAG measure for multimodal comparison using DeepBrainNet, a pretrained publicly available neural network. This comparison was performed to test whether a novel metric of white matter microstructure is corroborated by more established morphological methods. Statistical analysis (bottom row) included 3 main parts. First, the primary hypothesis that brain aging is accelerated in PWH was tested by modeling the DTI-derived BAG as an age × viral load interaction in multiple linear regression. Second, the association between BAG and cognition was assessed. Finally, additional potential risk factors for accelerated brain aging including comorbidities were explored.

in 626 normative participants (age = 55.0 [SD 18.4] years, range = 18.5–88.9; sex = 50% female). CamCAN images were also acquired on a Siemens 3.0 Tesla scanner, with TR/TE = 9100/104 ms, resolution =  $2 \times 2 \times 2$  mm, 30 gradient directions, and b-values from 0 to 2000 s/mm<sup>2</sup>. FA and MD were extracted from white matter ROIs as described above.

### Machine Learning

The MATLAB 2021a Regression Learner toolkit was used to train a model of brain predicted age, in which DTI scalar features were used to estimate age. Training data consisted of FA and MD from CamCAN, testing data were FA and MD from previously unseen study participants (PWH, controls).

A Gaussian process regression model was trained to predict age from FA and MD, standardized before training. The covariance kernel function was selected from among the following: rational quadratic, exponential, squared exponential, Matern-5/2, and Matern-3/2. An exponential kernel was chosen based on error minimization in cross-validation. The kernel is described by

$$k(x_i, x_j) = \sigma_f^2 \exp\left(-\frac{r}{\sigma_l}\right),$$

where  $r$  is the Euclidian distance between inputs  $x_i$  and  $x_j$ . Signal standard deviation  $\sigma_f$  was set to the standard deviation of the response variable (age) divided  $\sqrt{2}$ , and the characteristic length scale  $\sigma_l$  was initialized as the mean standard deviation of the DTI features. A constant basis function was used, with exact fitting and prediction methods.

Ten-fold cross-validation was used to assess accuracy. The trained model was then applied to the testing set, and the residuals (ie, BAG) were linearly detrended on age [29] and preserved for statistical analysis.

### Feature Ranking

To assess the relative importance of regional FA and MD features, a Relief regression algorithm was applied (*relieff*, MATLAB), producing a ranked ordering of ROIs by relative importance (feature weight). A  $k$ -nearest-neighbors approach was taken to identify DTI features that strongly predicted BAG in the study population.

### Multimodal Comparison

To determine whether white matter-derived BAG was consistent with established measures of brain predicted age, a publicly available deep learning model was applied to T<sub>1</sub>-weighted structural MRI. DeepBrainNet is a 2-dimensional convolutional neural net trained on 11 729 normative participants across multiple sites and scanners [30]. DeepBrainNet has previously been applied to estimate BAG from volumetric features in PWH, providing evidence of accelerated aging [20].

The goal of this step was to test whether BAG from our in-house DTI model correlated with volumetric changes in the same participants measured with a different MRI modality. T<sub>1</sub>-weighted MRI reflects alterations in the volume and shape of gray matter, white matter, and cerebrospinal fluid compartments, frequently occurring in parallel with white matter microstructural changes. If DTI-derived BAG values represent random residuals unrelated to pathology, they would not be expected to correlate with BAG from DeepBrainNet.

### Statistics and Hypothesis Testing

Demographic and clinical variables were compared between study groups (HIV-negative controls; PWH with undetectable VL; PWH with detectable VL) using 1-way ANOVAs. Two-tailed  $t$  tests were used for comparisons exclusive to the 2 subgroups of PWH.  $\chi^2$  tests were used for categorical variables.

The primary hypothesis specified that white matter aging is accelerated in older PWH with detectable VL compared to those with undetectable VL or HIV-negative controls. To test this, generalized linear regression was applied, with BAG as the response variable. Age, race, and sex were modeled as covariates due to group difference in these potential confounds.

Next, we tested for associations between white matter BAG and cognitive function in PWH, and for moderating effects of VL. We hypothesized that BAG is associated with cognitive performance in PWH, and that detectable VL would increase susceptibility to BAG-related cognitive impairment (modeled as a BAG  $\times$  VL interaction on global z-score).

The final objective was to identify comorbid risk factors, other than age and VL, associated with heterogeneous brain aging among PWH. Age, VL, race, and sex were therefore regressed out of BAG. This adjusted BAG was used to define subgroups: PWH with adjusted BAG  $>1.0$  standard deviation (SD) above the mean were classified as having pathological aging, while those with adjusted BAG  $\leq +1.0$  SD were defined as having typical or resilient aging. Membership in the pathological aging HIV subgroup was modeled with logistic regression on the following predictors: current CD4, nadir CD4, hepatitis C, body mass index, and 10-year Framingham cardiovascular risk score. This analysis was intended to be exploratory and hypothesis generating.

## RESULTS

### Participants

In total, 455 adult participants provided informed consent and participated in imaging and neuropsychological testing: 290 PWH (age = 48.2 [SD 13.7] years; 23% female; 65% African American) and 165 HIV-negative controls (age = 37.5 [SD 16.3] years; 47% female; 56% African American); 85% of PWH ( $n = 246$ ) had undetectable plasma VL and 15% ( $n =$

**Table 1. Demographic and Clinical Data**

Characteristic	HIV-Negative Controls	PWH Undetectable VL	PWH Detectable VL	<i>P</i> Value
No.	165	246	44	...
Age, y	37.5 (16.3)	49.0 (13.1)	44.1 (16.7)	<.001
Sex, female, No. (%)	77 (46.7)	60 (24.4)	8 (18.2)	<.001
Race, African American, No. (%)	92 (55.8)	156 (63.4)	32 (72.7)	.08
Education, y	13.8 (2.4)	13.3 (2.8)	13.0 (2.0)	.06
Body mass index	26.4 (5.7)	27.0 (6.1)	25.7 (5.3)	.34
Global cognitive z-score	-0.05 (0.63)	-0.32 (0.56)	-0.48 (0.84)	<.001
Viral load, copies/mL, log <sub>10</sub>	...	1.3 (0.09)	3.4 (1.2)	...
HIV duration, mo	...	178.1 (112.5)	108.6 (108.4)	<.001
ART duration, mo	...	173.0 (104.5)	155.7 (98.5)	.51
Most recent CD4 count, cells/μL	...	610.3 (314.2)	406.0 (345.4)	<.001
Nadir CD4 count, cells/μL	...	156.2 (183.7)	205.0 (211.4)	.17
CD4/CD8 ratio	...	0.81 (0.50)	0.41 (0.25)	<.001
Hepatitis C infection, No. (%)	...	21 (8.5)	3 (6.8)	.70
10-year Framingham risk score	...	16.4 (12.4)	21.5 (9.3)	.03

Data are mean (SD) except where indicated. *P* values are from 1-way analysis of variance (ANOVA) for continuous variables with 3 groups, 2-tailed *t* tests for continuous variables with 2 groups, and  $\chi^2$  tests for categorical variables.

Abbreviations: ART, antiretroviral therapy; HIV, human immunodeficiency virus; PWH, persons with HIV.

44) had detectable VL at admission. These subgroups were considered independently.

Demographics and clinical variables comprise [Table 1](#). Participant subgroups differed in age ( $P < .001$ ) and sex ( $P < .001$ ), but not race ( $P = .08$ ). These demographic factors may confound neuroimaging measures of brain predicted age, and were thus included as covariates in all subsequent analyses. Participant subgroups were not different in body mass index or education.

Compared to those with undetectable VL, PWH with detectable VL had significantly shorter disease duration ( $P < .001$ ), lower CD4 cell counts ( $P < .001$ ), lower CD4/CD8 ratios ( $P < .001$ ), and greater 10-year Framingham cardiovascular risk scores ( $P = .03$ ). Subgroups were similar in ART duration, nadir CD4 counts, and hepatitis C infection rates (all  $P > .05$ ).

### Brain Predicted Age

In the training dataset of 626 normative individuals, our DTI model estimated age with a mean absolute error (MAE) of 5.3 years in cross-validation. This model was then applied to study participants including PWH and controls. In the study cohort, the model predicted age with MAE = 12.8 years before linear detrending, and 5.1 years after this standard correction [29].

### Multimodal Comparison

BAG values derived from white matter FA and MD were significantly correlated with BAG values from volumetrics (T<sub>1</sub>-weighted MRI) obtained with DeepBrainNet ( $R = 0.38$ ;  $P < .001$ ). This relationship held in controls and PWH, regardless of VL ([Supplementary Figure 1](#)).

### Brain-Age Gap Is Accelerated in PWH With Detectable VL

Controlling for main effects of age, sex, and race, there was a significant overall age  $\times$  group interaction on BAG ( $F = 3.54$ ;  $P = .030$ ). In post hoc testing, PWH with detectable VL accumulated a mean of +1.5 years (95% confidence interval, .26–2.8 years) of BAG/decade compared to controls ( $P = .018$ ; [Figure 2](#) and [Table 2](#)). PWH with undetectable VL showed intermediate aging, accumulating +0.86 years BAG/decade compared to controls. However, this fell short of statistical significance ( $P = .052$ ).

### Feature Ranking

DTI scalars from white matter ROIs contributed differently to BAG estimation. The Relief algorithm ranked each ROI according to its weight, normalized to the top-ranked feature ([Figure 3](#)). For FA, the top 4 ROIs were corona radiata (weight = 1.0), internal capsule (0.47), external capsule (0.33), and fornix (0.27). For MD, top ROIs were fornix (1.0), corticospinal tract (0.68), internal capsule (0.64), and frontal-occipital fasciculus (0.54). As expected, global mean white matter FA was negatively correlated with BAG, while MD was positively correlated ([Supplementary Figure 2](#)).

### Cognitive Impairment and Viral Load

Because detectable VL was correlated with accelerated white matter aging, we hypothesized that the BAG-cognition relationship is VL dependent. To test this, global cognitive z-score was modeled as a BAG  $\times$  VL interaction, controlling for age, sex, and race. VL was found to be a significant moderator: BAG was negatively associated with cognitive z-score in PWH with detectable VL but not those with undetectable VL ( $P < .001$ ; [Figure 4](#)).

### BAG Is Associated With Cardiovascular Risk in PWH

Pathological aging was defined as a demographically adjusted BAG  $> 1.0$  SD, or 6.4 years above the mean. Pathological aging was modeled using logistic regression with univariate predictors. Of 5 predictors considered, only 10-year Framingham cardiovascular score ( $P = .027$ ) was associated with pathological aging, indicating an increase in brain predicted age with greater cardiovascular risk.

## DISCUSSION

In this neuroimaging study, machine learning quantified microstructural integrity of white matter in PWH and

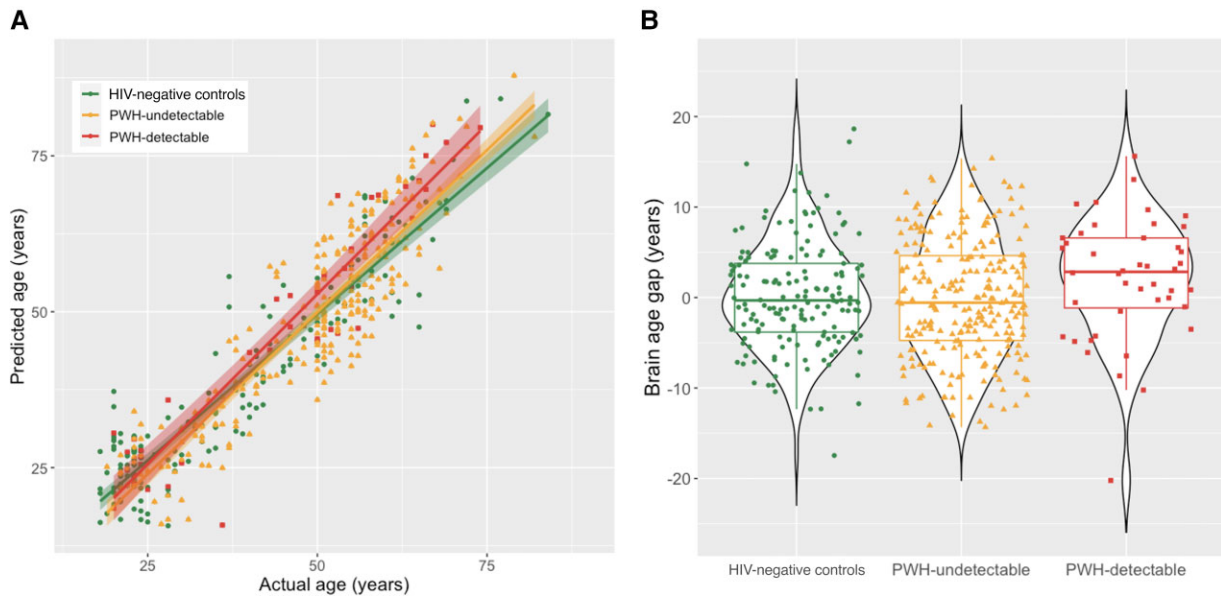


**Figure 2.** Age and viral load effects on white matter brain age gap. *A*, Participant chronological ages ( $x$ ) are plotted against brain predicted ages ( $y$ ) for HIV-negative controls (circles), persons with HIV (PWH) with undetectable viral load (VL; triangles), and PWH with detectable VL (squares). Shaded areas represent 95% confidence intervals. PWH with detectable VL have increased BAG with age vs HIV-negative controls or PWH with undetectable VL (interaction  $P = .018$ ). PWH with undetectable VL showed an intermediate effect that was not statistically significant (interaction  $P = .052$ ). *B*, Violin and box plots of the BAG for each study group across all ages. For box plots, central horizontal line represents the median, box boundaries are quartiles 1 and 3, and whiskers extend to minimum and maximum non-outlier values. For violin plots, plot width represents probability density of datapoints across the range of BAG.

seronegative controls through estimation of the BAG, obtained by modeling a normative relationship between age and DTI. This model was subsequently applied to a large cohort of previously unseen study participants ( $n = 455$ ) including PWH and HIV-negative controls. The DTI-derived BAG was compared with a well-established deep learning model of volumetric BAG, with congruent results [30].

DTI-derived BAG was increased in older PWH with detectable VL, indicating a disparity between chronological age and white matter-specific brain age (Figure 2). This gap was not present in controls, PWH with undetectable VL, or younger participants of either serostatus. This finding demonstrates accelerated pathological changes to white matter microstructure in at-risk subpopulations of PWH, and is consistent with an emerging literature on brain aging with HIV [2, 19, 20]. There is some disagreement about whether this elevation represents a fixed accentuation over the lifespan, or an acceleration that widens with age [31]. Our results are consistent with the latter, as BAG was increased in older but not younger individuals with detectable VL.

Interpretation of this finding is complicated by alternative explanations. Increased BAG may represent true acceleration, where suboptimal viral suppression causes inflammation and cumulative white matter degradation. The magnitude of pathological effects may be small enough that accreted differences only become detectable later in life. Alternatively, this apparent

acceleration may represent a latent cohort effect, where older PWH were exposed to a more risk factors than their younger peers in the cART era. Our cross-sectional findings cannot absolutely distinguish between these possibilities, which are not mutually exclusive.

However, previous work on longitudinal white matter changes may contextualize our results. A recent DTI study with 4-year follow-up observed that PWH had greater MD increases compared to controls, associated with cognitive decline in older PWH [32]. In contrast, another study of PWH on stable cART found no DTI changes at 2-year median follow-up [33]. Other studies have examined longitudinal relationships between white matter and cognition. For example, intraindividual variability on neuropsychological performance increased more for PWH than controls over 2 years. Neuropsychological changes in PWH were also associated with lower FA in 2 white matter tracts [34].

White matter health can also be quantified volumetrically, as in a longitudinal study of PWH over age 60 years, which found no significant changes in white matter volume at mean follow-up of 3.4 years [35]. However, an earlier study did find white matter loss in ART-treated PWH, even with viral suppression [36]. These varying results may be due to modest rates of change combined with limited sample sizes ( $n = 20-40$ ). In contrast, our cross-sectional analysis covers a much longer time scale and utilizes a larger cohort.

**Table 2. Effects and Significance for Primary Hypothesis Testing**

PWH Undetectable vs HIV-Negative Controls		PWH Detectable vs HIV-Negative Controls		PWH Detectable vs PWH Undetectable	
Effect	P Value	Effect	P Value	Effect	P Value
+0.86 y BAG/decade	.052	+1.5 y BAG/decade	.018*	+0.68 y BAG/decade	.30

The hypothesis of accelerated aging in PWH with detectable VL was tested using an interaction model:  $BAG \sim age \times group + covariates$ , with 3 groups: HIV-negative controls, PWH with undetectable VL, and PWH with detectable VL. Effects were quantified as the linear slope of BAG increase per decade. PWH with detectable VL were found to have a significantly faster increase in BAG than controls ( $P = .018$ ) while those with undetectable VL were not significantly different ( $P = .052$ ). \* $P < .05$ .

Abbreviations: BAG, brain age gap; HIV, human immunodeficiency virus; PWH, persons with HIV; VL, viral load.

In this study, PWH with undetectable VL had acceleration intermediate between PWH with detectable VL and controls. While this effect did not achieve our predefined threshold for significance ( $P = .052$ ), its magnitude (+0.86 years BAG/decade) is sufficient to merit further investigation. Notably, previous findings on brain structure identified accelerated aging in PWH with both detectable and undetectable VL [20], with an apparent gradation of pathology with VL. Accelerated aging in virally suppressed PWH may represent a legacy of acute infection, or ongoing HIV replication in the central nervous system even when suppressed in plasma.

Spatial patterns of white matter change were heterogeneous, as indicated by differential contributions of ROIs to BAG estimation. In general, greater weight was assigned to deep white matter near the basal ganglia and limbic system, such as the

internal capsule and fornix. Cortical white matter including the corona radiata and frontal-occipital fasciculus also influenced BAG, suggesting that accelerated aging is distributed (Figure 3). Notably, tract weights for FA and MD differed spatially, possibly indicating spatial difference for different types of HIV-related white matter pathology—for example, axonal degeneration, gliosis, or demyelination. Further studies are needed to verify such differences.

The fornix, the major output tract of the hippocampus, is a marker of chronic HIV-related injury [16], and its atrophy predicts cognitive impairment in older adults [37]. Hippocampal shrinkage may confound DTI measures in this region; however, Calon et al [16] found that fornix FA and MD were altered in PWH with cardiovascular disease after controlling for hippocampal volume.

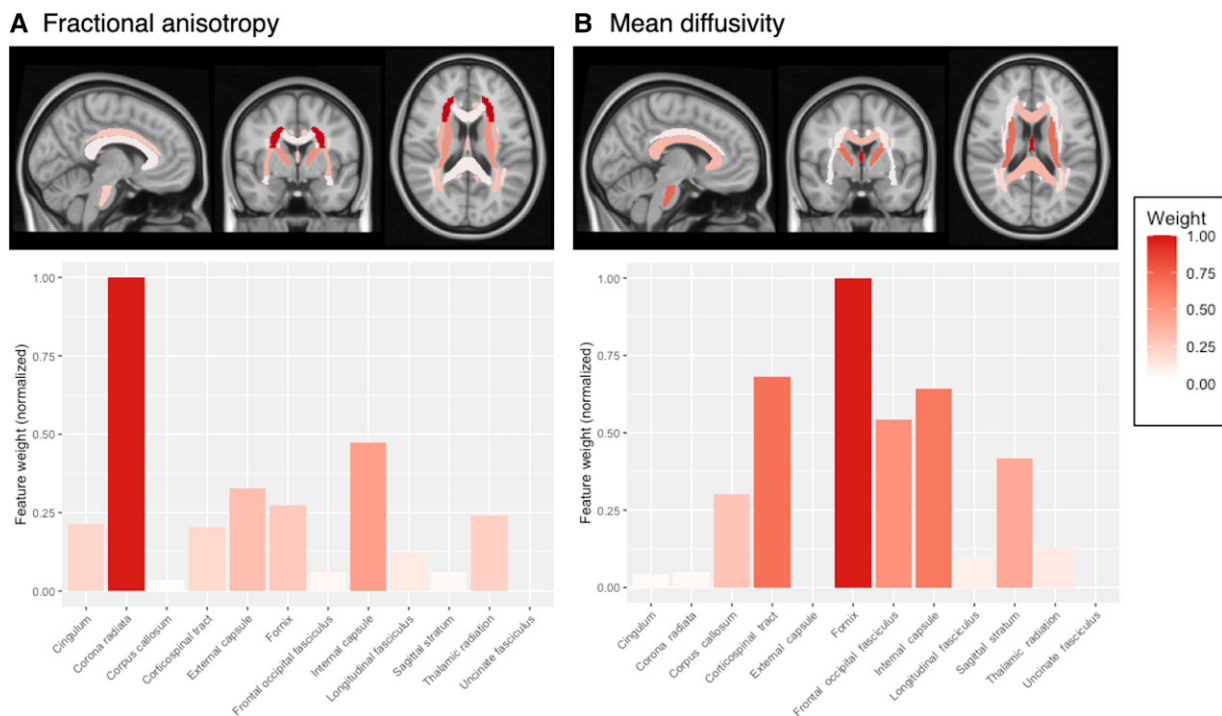


**Figure 3.** Region-of-interest weights in brain-age gap (BAG) estimation. A Relief regression algorithm was applied to identify diffusion tensor imaging (DTI) features that most strongly predict the BAG. Twelve bilateral white matter regions of interest were included, and their relative weights were normalized to the most important feature (fixed at 1.0). Fractional anisotropy (FA, A) and mean diffusivity (MD, B) were analyzed separately. Two of the top 4 features for FA and MD were shared in common: the internal capsule and fornix.

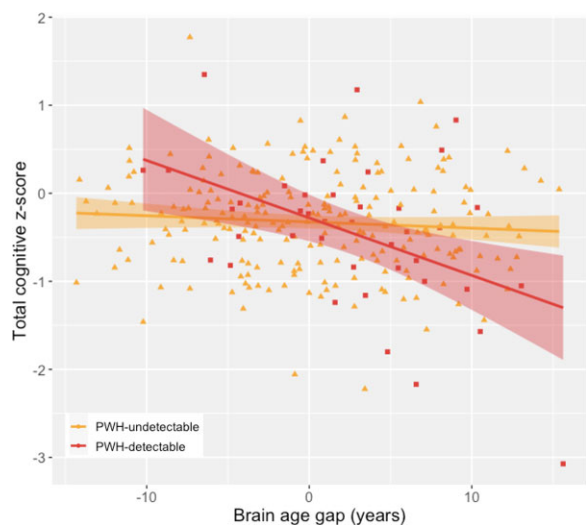


**Figure 4.** Cognition is correlated with brain age gap (BAG) in people with detectable HIV. Global cognitive function was assessed with a 15-instrument battery. Raw scores were converted to z-scores with adjustment for age, sex, race, and education following normative procedures. An inverse relationship between global cognitive z-score and BAG was observed for persons with HIV (PWH) who had detectable viral load (VL; squares) but not PWH with undetectable VL (triangles), constituting a significant interaction ( $P < .001$ ). The effect remains significant with removal of the high-leverage point at bottom right.

Differences between older PWH and controls were small compared to total BAG variability among PWH, indicating that heterogeneous brain aging may depend on other predictors of risk or resilience. We therefore performed an exploratory analysis to identify potentially important factors. Among PWH, pathologically elevated BAG ( $>6.4$  years) was significantly associated with elevated 10-year Framingham cardiovascular risk. By contrast, pathological BAG was not associated with traditional risk factors such as T lymphocytes.

Non-HIV comorbidities are a subject of increasing emphasis, because age and VL are insufficient to account for the full phenotypic spectrum. Cardiovascular disease is a major cause of morbidity and mortality in PWH, and is connected to neuropathology through shared inflammatory pathways [38]. Vascular disease is especially salient to PWH, who are at increased risk for stroke [39], diminished cerebrovascular reactivity [40], and vascular cognitive impairment [41]. The presence of preexisting cardiovascular disease [42], insulin resistance [43], abnormal glucose metabolism [44], and abdominal obesity [45] have all been linked with neurocognitive disorders or brain imaging abnormalities in PWH. Our finding of an association between Framingham score and pathological white matter BAG suggests that mitigation of cerebrovascular risk may be crucial for resilient aging in PWH.

The measured relationship between white matter microstructure and cognition has varied. Some reports have indicated that DTI reflects global impairment [46, 47] or

domain-specific function [2], while others have found little association [3]. Here, the relationship between white matter aging and cognition was examined with respect to VL. Persons with detectable HIV were shown to drive the negative relationship between BAG and cognition, with the greatest impairment in those with both detectable VL and increased BAG (Figure 4).

This may indicate that PWH with undetectable VL have greater cognitive reserve, as neuropsychological performance in this subgroup is less sensitive to microstructural damage. Previous studies have found that cognitive reserve is diminished in older PWH with cognitive impairment [48], but may be maintained with viral suppression [49].

These results should be considered in light of some limitations. Substance abuse is a major contributor to poor neurological health in PWH, but this study was not designed to assess its role. cART neurotoxicity was also not considered, despite evidence linking specific classes of ART to structural changes [50]. Additionally, neuropsychological domains beyond cognition such as negative valence or social systems were not considered. Finally, we sought to compare our findings with an external, well-validated BAG model. However, to our knowledge there are no publicly available DTI-based brain age models, while  $T_1$ -weighted MRI approaches are more developed. Moreover, volumetric deep learning models rely on minimally processed images, whereas DTI requires extensive preprocessing, and is very sensitive to postacquisition procedures (denoising, tract mapping, parcellation), which may limit generalizability.

In conclusion, both nonmodifiable and modifiable risk factors likely impact the development of age-like white matter changes in PWH over the lifespan. These findings also highlight the heterogeneity of neurocognitive outcomes in older PWH, underscoring the need to better characterize biological subtypes of neurological HIV infection.

#### Supplementary Data

Supplementary materials are available at *The Journal of Infectious Diseases* online (<http://jid.oxfordjournals.org/>). Supplementary materials consist of data provided by the author that are published to benefit the reader. The posted materials are not copyedited. The contents of all supplementary data are the sole responsibility of the authors. Questions or messages regarding errors should be addressed to the author.

#### Notes

**Acknowledgments.** We are grateful to all participants for making this study possible. Data used in the preparation of this work were obtained from the Cambridge Centre for Ageing and Neuroscience ([cam-can.org](http://cam-can.org)). Diffusion tensor image preprocessing utilized ENIGMA-DTI protocols ([enigma.ini.usc.edu/protocols/dti-protocols](http://enigma.ini.usc.edu/protocols/dti-protocols)). DeepBrainNet is accessible at ([github.com/vishnubashyam/DeepBrainNet](https://github.com/vishnubashyam/DeepBrainNet)). We



acknowledge Vishnu Bashyam, Talia Nir, and Neda Jahanshad for assistance with these toolkits.

**Disclaimer.** The content is solely the responsibility of the authors and does not necessarily represent the official views of the National Institutes of Health

**Financial support.** The work was supported by the National Institute of Mental Health (grant numbers R01MH118031 and F32MH129151); and the National Institute of Nursing Research (grant numbers R01NR015738, R01NR012907, R01NR012657, and R01NR014449). CamCAN funding was provided by the UK Biotechnology and Biological Sciences Research Council (grant number BB/H008217/1), together with support from the UK Medical Research Council and University of Cambridge, UK.

**Potential conflicts of interest.** The authors: No reported conflicts of interest. All authors have submitted the ICMJE Form for Disclosure of Potential Conflicts of Interest. Conflicts that the editors consider relevant to the content of the manuscript have been disclosed.

## References

1. Horvath S, Levine AJ. HIV-1 infection accelerates age according to the epigenetic clock. *J Infect Dis* **2015**; 212:1563–73.
2. Kuhn T, Kaufmann T, Doan NT, et al. An augmented aging process in brain white matter in HIV. *Hum Brain Mapp* **2018**; 39:2532–40.
3. Su T, Caan MWA, Wit FWNM, et al. White matter structure alterations in HIV-1-infected men with sustained suppression of viraemia on treatment. *AIDS* **2016**; 30:311–22.
4. Seider TR, Gongvatana A, Woods AJ, et al. Age exacerbates HIV-associated white matter abnormalities. *J Neurovirol* **2016**; 22:201–12.
5. Zhu T, Zhong J, Hu R, et al. Patterns of white matter injury in HIV infection after partial immune reconstitution: a DTI tract-based spatial statistics study. *J Neurovirol* **2013**; 19:10–23.
6. Stubbe-Drger B, Deppe M, Mohammadi S, et al. Early microstructural white matter changes in patients with HIV: a diffusion tensor imaging study. *BMC Neurol* **2012**; 12:1–10.
7. Kuhn T, Jin Y, Huang C, et al. The joint effect of aging and HIV infection on microstructure of white matter bundles. *Hum Brain Mapp* **2019**; 40:4370–80.
8. Cole JH, Poudel RPK, Tsagkrasoulis D, et al. Predicting brain age with deep learning from raw imaging data results in a reliable and heritable biomarker. *NeuroImage* **2017**; 163:115–24.
9. Becker JT, Maruca V, Kingsley LA, et al. Factors affecting brain structure in men with HIV disease in the post-HAART era. *Neurorad* **2012**; 54:113–21.
10. Underwood J, Cole JH, Leech R, et al. Multivariate pattern analysis of volumetric neuroimaging data and its relationship with cognitive function in treated HIV disease. *J Acquir Immune Defic Syndr* **2018**; 78:429–36.
11. Sanford R, Cruz ALF, Scott SC, et al. Regionally specific brain volumetric and cortical thickness changes in HIV-infected patients in the HAART era. *J Acquir Immune Defic Syndr* **2017**; 74:563–70.
12. O'Connor EE, Zeffiro TA, Zeffiro TA. Brain structural changes following HIV infection: meta-analysis. *Am J Neuroradiol* **2018**; 39:54–62.
13. Autenrieth CS, Beck EJ, Stelzle D, Mallouris C, Mahy M, Ghys P. Global and regional trends of people living with HIV aged 50 and over: estimates and projections for 2000–2020. *PLoS One* **2018**; 13:e0207005.
14. Valcour VG. HIV, aging, and cognition: emerging issues. *Top Antivir Med* **2013**; 21:119.
15. Rodriguez-Penney AT, Iudicello JE, Riggs PK, et al. Co-morbidities in persons infected with HIV: increased burden with older age and negative effects on health-related quality of life. *AIDS Patient Care Stds* **2013**; 27:5–16.
16. Calon M, Menon K, Carr A, et al. Additive and synergistic cardiovascular disease risk factors and HIV disease markers' effects on white matter microstructure in virally suppressed HIV. *J Acquir Immune Defic Syndr* **2020**; 84:543–51.
17. Cole JH, Ritchie SJ, Bastin ME, et al. Brain age predicts mortality. *Mol Psychiatry* **2018**; 23:1385–92.
18. Gaser C, Franke K, Klöppel S, Koutsouleris N, Sauer H. BrainAGE in mild cognitive impaired patients: predicting the conversion to Alzheimer's Disease. *PLoS One* **2013**; 8:e67346.
19. Cole JH, Underwood J, Caan MWA, et al. Increased brain-predicted aging in treated HIV disease. *Neurology* **2017**; 88:1349–57.
20. Petersen KJ, Metcalf N, Cooley S, et al. Accelerated brain aging and cerebral blood flow reduction in persons with HIV. *Clin Infect Dis* **2021**; 73:1813–21.
21. Wilson PWF, D'Agostino RB, Levy D, Belanger AM, Silbershatz H, Kannel WB. Prediction of coronary heart disease using risk factor categories. *Circulation* **1998**; 97:1837–47.
22. Buuren SV, Groothuis-Oudshoorn K. mice: Multivariate imputation by chained equations in R. *J Stat Softw* **2011**; 45:1–67.
23. Urowitz MB, Ibañez D, Su J, Gladman DD. Modified Framingham risk factor score for systemic lupus erythematosus. *J Rheumatol* **2016**; 43:875–9.
24. Kang T, Kraft P, Gauderman WJ, Thomas D. Multiple imputation methods for longitudinal blood pressure

- measurements from the Framingham Heart Study. *BMC Genet* **2003**; 4:1–5.
25. Paul RH, Cooley SA, Garcia-Egan PM, Ances BM. Cognitive performance and frailty in older HIV-positive adults. *J Acquir Immune Defic Syndr* **2018**; 79:375–80.
  26. Kochunov P, Hong LE, Dennis EL, et al. ENIGMA-DTI: Translating reproducible white matter deficits into personalized vulnerability metrics in cross-diagnostic psychiatric research. *Hum Brain Mapp* **2020**; 43:194–206.
  27. Taylor JR, Williams N, Cusack R, et al. The Cambridge centre for ageing and neuroscience (Cam-CAN) data repository: Structural and functional MRI, MEG, and cognitive data from a cross-sectional adult lifespan sample. *Neuroimage* **2017**; 144:262–9.
  28. Shafto MA, Tyler LK, Dixon M, et al. The Cambridge Centre for Ageing and Neuroscience (CamCAN) study protocol: a cross-sectional, lifespan, multidisciplinary examination of healthy cognitive ageing. *BMC Neurol* **2014**; 14:204.
  29. Le TT, Kuplicki RT, McKinney BA, et al. A nonlinear simulation framework supports adjusting for age when analyzing BrainAGE. *Front Aging Neurosci* **2018**; 10:317.
  30. Bashyam VM, Erus G, Doshi J, et al. MRI signatures of brain age and disease over the lifespan based on a deep brain network and 14 468 individuals worldwide. *Brain* **2020**; 143:2312–24.
  31. Pathai S, Bajjlan H, Landay AL, High KP. Is HIV a model of accelerated or accentuated aging? *J Gerontol A Biol Sci Med Sci* **2014**; 69:833–42.
  32. Haynes BI, Pitkanen M, Kulasegaram R, et al. HIV: ageing, cognition and neuroimaging at 4-year follow-up. *HIV Med* **2018**; 19:376–85.
  33. Corrêa DG, Zimmermann N, Tukamoto G, et al. Longitudinal assessment of subcortical gray matter volume, cortical thickness, and white matter integrity in HIV-positive patients. *J Magn Reson Imaging* **2016**; 44:1262–9.
  34. Jones JD, Kuhn T, Mahmood Z, Singer EJ, Hinkin CH, Thames AD. Longitudinal intra-individual variability in neuropsychological performance relates to white matter changes in HIV. *Neuropsychology* **2018**; 32:206.
  35. Clifford KM, Samboju V, Cobigo Y, et al. Progressive brain atrophy despite persistent viral suppression in HIV over age 60. *J Acquir Immune Defic Syndr* **2017**; 76:289.
  36. Cardenas VA, Meyerhoff DJ, Studholme C, et al. Evidence for ongoing brain injury in human immunodeficiency virus-positive patients treated with antiretroviral therapy. *J Neurovirol* **2009**; 15:324–33.
  37. Fletcher E, Raman M, Huebner P, et al. Loss of fornix white matter volume as a predictor of cognitive impairment in cognitively normal elderly individuals. *JAMA Neurol* **2013**; 70:1389–95.
  38. Miller CJ, Baker JV, Bormann AM, et al. Adjudicated morbidity and mortality outcomes by age among individuals with HIV infection on suppressive antiretroviral therapy. *PLoS One* **2014**; 9:e95061.
  39. Chow FC, Regan S, Feske S, Meigs JB, Grinspoon SK, Triant VA. Comparison of ischemic stroke incidence in HIV-infected and non-HIV-infected patients in a US health care system. *J Acquir Immune Defic Syndr* **2012**; 60:351–8.
  40. Callen AL, Dupont SM, Pyne J, et al. The regional pattern of abnormal cerebrovascular reactivity in HIV-infected, virally suppressed women. *J Neurovirol* **2020**; 26:734–42.
  41. Cysique LA, Brew BJ. Vascular cognitive impairment and HIV-associated neurocognitive disorder: a new paradigm. *J Neurovirol* **2019**; 25:710–21.
  42. Wright EJ, Grund B, Robertson K, et al. Cardiovascular risk factors associated with lower baseline cognitive performance in HIV-positive persons. *Neurology* **2010**; 75:864–73.
  43. Valcour VG, Sacktor NC, Paul RH, et al. Insulin resistance is associated with cognition among HIV-1-infected patients: the Hawaii Aging With HIV cohort. *J Acquir Immune Defic Syndr* **2006**; 43:405–10.
  44. Nakamoto BK, Jahanshad N, McMurtray A, et al. Cerebrovascular risk factors and brain microstructural abnormalities on diffusion tensor images in HIV-infected individuals. *J Neurovirol* **2012**; 18:303–12.
  45. Sattler F, Jiaxiu HE, Letendre S, et al. Abdominal obesity contributes to neurocognitive impairment in HIV infected patients with increased inflammation and immune activation. *J Acquir Immune Defic Syndr* **2015**; 68:281.
  46. Cysique LA, Soares JR, Geng G, et al. White matter measures are near normal in controlled HIV infection except in those with cognitive impairment and longer HIV duration. *J Neurovirol* **2017**; 23:539–47.
  47. Chang L, Wong V, Nakama H, et al. Greater than age-related changes in brain diffusion of HIV patients after 1 year. *J Neuroimmune Pharmacol* **2008**; 3:265–74.
  48. Chang L, Holt JL, Yakupov R, Jiang CS, Ernst T. Lower cognitive reserve in the aging human immunodeficiency virus-infected brain. *Neurobiol Aging* **2013**; 34:1240–53.
  49. Milanini B, Ciccarelli N, Fabbiani M, et al. Cognitive reserve and neuropsychological functioning in older HIV-infected people. *J Neurovirol* **2016**; 22:575–83.
  50. O'Halloran JA, Cooley SA, Strain JF, et al. Altered neuropsychological performance and reduced brain volumetrics in people living with HIV on integrase strand transfer inhibitors. *AIDS* **2019**; 33:1477–83.